doi:10.1016/j.jmb.2004.08.102 J. Mol. Biol. (2004) 343, 1269–1280

JMB

Available online at www.sciencedirect.com

SCIENCE DIRECT®

ELSEVIER

The Origin of Enantioselectivity in Aldolase Antibodies: Crystal Structure, Site-directed Mutagenesis, and Computational Analysis

Xueyong Zhu[1,2], Fujie Tanaka[1,2,3], Yunfeng Hu[1], Andreas Heine[1] Roberta Fuller[1,2,3], Guofu Zhong[1,2], Arthur J. Olson[1], Richard A. Lerner[1,2,3] Carlos F. Barbas III[1,2,3]* and Ian A. Wilson[1,2]*

[1]*Department of Molecular Biology, The Scripps Research Institute, 10550 North Torrey Pines Road, La Jolla, CA 92037 USA*

[2]*The Skaggs Institute for Chemical Biology, The Scripps Research Institute, 10550 North Torrey Pines Road, La Jolla CA 92037, USA*

[3]*Department of Chemistry The Scripps Research Institute 10550 North Torrey Pines Road La Jolla, CA 92037, USA*

**Corresponding authors*

Catalytic aldolase antibodies, generated by reactive immunization, catalyze the aldol reaction with the efficiency of natural enzymes, but accept a much broader range of substrates. Two separate groups of aldolase antibodies that catalyze the same aldol reactions with antipodal selectivity were analyzed by comparing their amino acid sequences with their crystal structures, site-directed mutagenesis data, and computational docking of the transition states of the aldol reaction. The crystal structure of aldolase antibody 93F3 Fab′ at 2.5 Å resolution revealed a combining site with two lysine residues, including LysL89 that reacts to form the covalent enamine intermediate. In contrast, antibody 33F12 has one active site lysine, LysH93. The reactive lysine residues in each group of antibodies are differentially located on the heavy and light chain variable regions in pseudo-symmetric opposite orientations, but both within highly hydrophobic environments. Thus, the defining feature for the observed enantioselectivities of these aldolase antibody catalysts is the respective location and relative disposition of the reactive lysine residues within the active sites of these catalysts.

Keywords: enantioselectivity; catalytic aldolase antibody; crystal structure; site-directed mutagenesis; covalent flexible protein docking

Introduction

Antibodies generated by reactive immunization with 1,3-diketone derivatives catalyze the aldol reaction, a basic carbon–carbon bond-forming reaction,[1–7] and have emerged as promising tools for selective chemotherapy through specific activation of prodrugs *in vitro* and *in vivo*.[8] These aldolase antibodies operate *via* an enamine mechanism, similar to natural class I aldolase enzymes, which utilize the uncharged ε-amino group of a reactive lysine residue in their active sites for the formation of an enamine, a carbon nucleophile (Scheme 1). These antibodies are the most efficient man-made designer protein catalysts to date with the efficiency of natural enzymes, but are more accepting of a much wider range of substrates. Their catalytic proficiency[9] ($(k_{cat}/K_m)/k_{uncat}$) can be greater than $10^{13}\ M^{-1}$.[6] The catalytic efficiency (k_{cat}/K_m) of one of these aldolase antibodies, antibody 93F3, in the retro-aldol reaction for the best substrate is $4.5\times 10^5\ s^{-1}\ M^{-1}$, which is tenfold greater than that of the best characterized aldolase enzyme,[10] fructose-1,6-biphosphate aldolase ($4.9\times 10^4\ s^{-1}\ M^{-1}$).

The reactions catalyzed by these various aldolase antibodies are highly enantioselective. According to the enantiopreferences of their catalyzed reactions, the aldolase antibodies can be divided into two groups: one group consists of antibodies 38C2, 33F12, 40F12 and 42F1 which catalyze the aldol reaction to afford (*S*)-**9** and catalyze the retro-aldol reaction of (*S*)-**9** (Scheme 1(b)), and the other includes antibodies 84G3 and 93F3 which catalyze the aldol reaction to produce (*R*)-**9** and catalyze the retro-aldol reaction of (*R*)-**9** (Scheme 1(b)).[1–7] Antibodies 38C2 and 33F12 were elicited against hapten **1**, while antibodies 40F12, 42F1, 84G3 and 93F3 were

Present address: A. Heine, Department of Pharmaceutical Chemistry, Philipps-University Marburg, Marbacher Weg 6, 35032 Marburg, Germany.

Abbreviations used: CDRs, complementarity determining regions; LGA, Lamarckian genetic algorithm.

E-mail addresses of the corresponding authors: wilson@scripps.edu; carlos@scripps.edu

generated with hapten **2** (Scheme 1(a)). Antipodal selectivities have also been achieved by other catalytic antibodies as, for example, abzymes that catalyze hydrolysis of either (*R*)- or (*S*)-esters.[11]

Here, we address questions about how these differences in enantioselectivity arise by evaluating the structural differences between these two groups of aldolase antibody catalysts. Although the diketone hapten **1** does not have a chiral center, antibodies generated using this hapten catalyze aldol reactions with antipodal enantioselectivities.[1,2] As antibody catalysts are man-made, such insights are critical for further development of these designer protein catalysts. We have reported the crystal structure of aldolase antibody 33F12,[2] and have now determined the crystal structure of aldolase antibody 93F3 possessing antipodal selectivity relative to 33F12. We have compared the structures of these two antibodies and the amino acid sequences of these two antibody families, and have used site-directed mutagenesis and computational docking analysis to determine the origins of the enantioselectivity of the antibody-catalyzed aldol reactions.

Results and Discussion

Comparison of aldolase antibody sequences

The amino acid sequences of various aldolase antibodies are shown in Figure 1. As reported, aldolase antibodies 38C2, 33F12, 40F12, and 42F1 possess the same enantioselectivity in their catalyzed reactions, share high amino acid sequence identity, and have a reactive lysine residue at H93.[12]

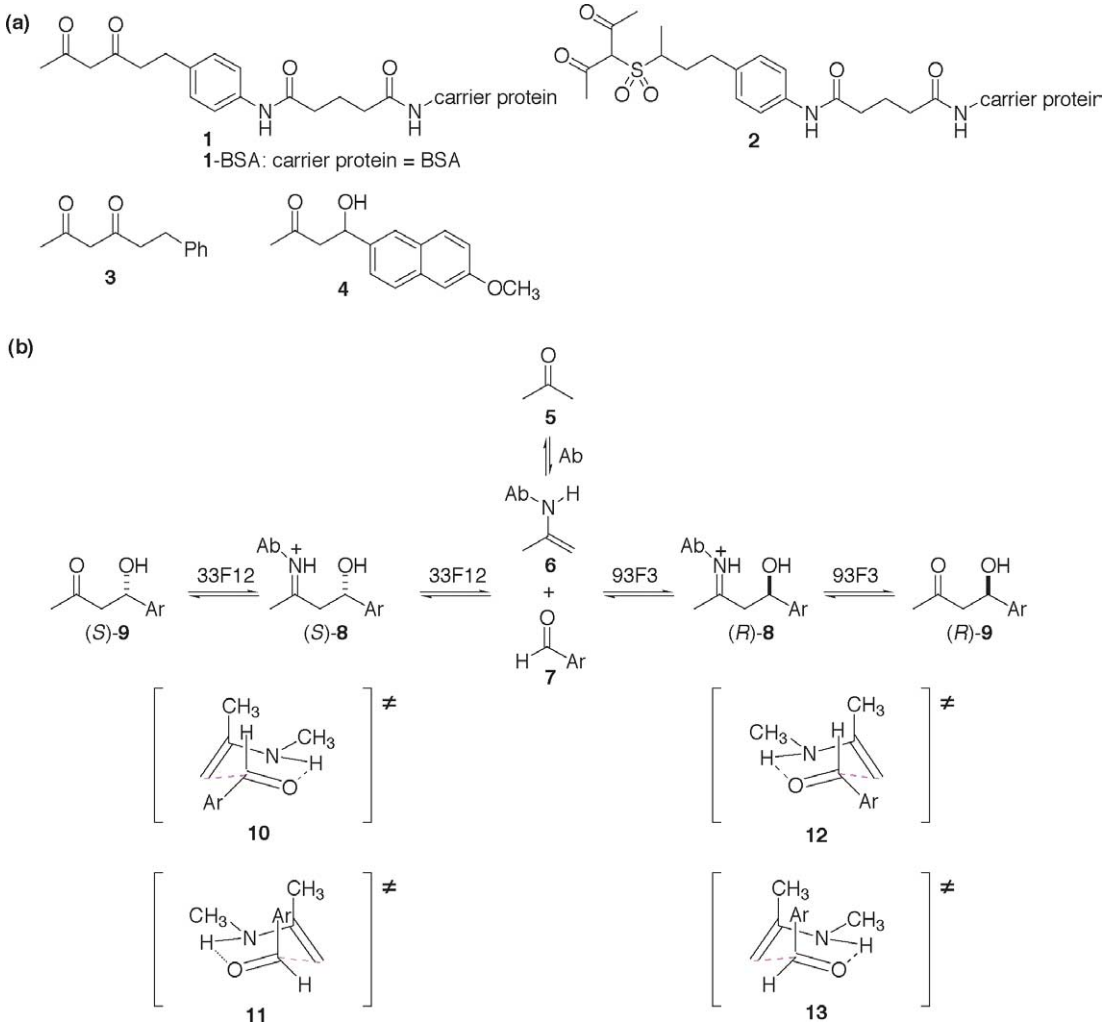

Scheme 1. (a) Diketone haptens **1** and **2** were used to elicit the aldolase antibodies by reactive immunization. Diketone **3** was used in the inhibition ELISA experiments. Aldol **4** was used in the catalytic assay. (b) Antibody-catalyzed aldol reaction of acetone **5** and aldehyde **7**. Antibody 33F12 predominately yields product (*S*)-**9**, while antibody 93F3 predominately yields product (*R*)-**9**. According to the results of quantum mechanical calculations (see Computational studies on the enantioselectivity of aldolase antibodies section and Figure 4), transition states **10** and **11** lead to (*S*)-**9**, while transition states **12** and **13** lead to (*R*)-**9**. Transition states **12** and **13** are mirror images of **10** and **11**, respectively. Methylamine was used (i.e. Ab = CH_3) in these schematic representations of transition states **10**–**13**. Aldehyde ArCHO = *p*-$(CH_3)_2CHCONHC_6H_4CHO$ was used in computational calculations. Newly forming C–C bonds are colored in pink.

Figure 1. Amino acid sequence alignment of antibodies 84G3 and 93F3 with other known aldolase antibodies. The complementarity determining regions (CDRs) are indicated and catalytic lysine residues are shown in red boxes. (a) V_L sequences and (b) V_H sequences.

Although the lengths of the light chain V_L CDR1 and the heavy chain V_H CDR3 of 40F12 and 42F1 are shorter than those of 38C2 and 33F12, the crystal structure analysis of 33F12 and the homology model of 40F12 indicate a similar hydrophobic active site.[12] Similarly, antibodies 84G3 and 93F3, generated by immunization with hapten **2**,[6] are highly homologous and differ from one another by only one amino acid substitution in the V_L domain and eight substitutions in the V_H domains. Antibodies 84G3 and 93F3 appear to originate from the same germline antibody. The sequence analysis also shows that antibodies 84G3 and 93F3 have the same number of lysine residues at the same positions in their variable domains. On the other hand, the amino acid sequences of 84G3 and 93F3 are very different from the aldolase antibody family that includes 38C2, 33F12, 40F12, and 42F1. Significantly, in 84G3 and 93F3, the essential lysine residue is at L89 (see below), while in the other family, the catalytic lysine is at H93. Thus, the antipodal selectivity of the two families is a result of selection

Table 1. Data collection and refinement statistics of 93F3 Fab′

Space group	$P2_12_12_1$
Unit cell parameters (Å)	$a=79.7$, $b=81.2$, $c=149.5$
Resolution (Å)	50.0–2.50 (2.59–2.50)[a]
No. of unique reflections	31,622
Redundancy	4.1
Average $I/\sigma(I)$	17.4 (3.5)[a]
Completeness	91.3 (83.7)[a]
R_{merge}[b]	0.088 (0.430)[a]
Refined residues	868
Refined water molecules	277
R_{cryst}[c]	0.233
R_{free}[d]	0.281
Average B-values (Å^2)	
Protein	53.4
Water molecules	51.2
Ramachandran plot (%)[e]	87.7, 11.3, 0.7, 0.3
RMSD bond lengths (Å)	0.011
RMSD bond angles (deg.)	1.6

[a] Parentheses denote outer-shell statistics.

[b] $R_{merge} = \sum_h \sum_i |I_i(h) - \langle I(h)\rangle| / \sum_h \sum_i I_i(h)$, where $\langle I(h)\rangle$ is the average intensity of i symmetry related observations of reflections with Bragg index h.

[c] $R_{cryst} = \sum_{hkl} |F_o - F_c| / \sum_{hkl} |F_o|$, where F_o and F_c are the observed and calculated structure factors.

[d] R_{free} was calculated as for R_{cryst}, but on 5% of data excluded before refinement.

[e] The values are percentages of residues in the most favored, additional allowed, generously allowed and disallowed regions. SerH128 in the disallowed region exhibits unusual main-chain torsion angle in a flexible loop. AlaL51 as expected shows unusual main-chain torsion angles (ϕ and ψ values of AlaL51 in two Fab molecules are 65.0°, −26.9° and 64.6°, −29.3°, respectively) in the generously allowed region, but in a well-defined γ-turn observed in almost all antibody structures.

of completely different amino acid sequences from the immune system antibody repertoire.

Structural characterization of antibody 93F3 Fab′

To understand the nucleophilic character of the reactive lysine within aldolase antibodies and to explore the structural basis for their enantioselectivity, the crystal structure of the Fab′ antigen binding fragment of antibody 93F3 (Table 1) was determined for comparison with our previous 33F12 structure.[2] 93F3 Fab′ has a γ_1 heavy chain and a κ light chain, and its overall structure is similar to other known Fab structures. A deep binding pocket is formed from the six light and heavy-chain complementarity determining regions (CDRs), denoted CDR L1, L2, L3, H1, H2 and H3, respectively (Figure 2). The entrance of the combining site of 93F3 is a narrow, elongated cleft (Figure 3(A)). The binding pocket is more than 10 Å deep, comparable to the combining sites of other anti-hapten antibodies. Two lysine residues are located at the bottom of the binding pocket; LysL89 is located in a hydrophobic environment, whereas LysL46 is in a hydrophilic environment (Figure 3(A)). A third lysine, LysH94, is located adjacent to CDR H3 loop, but its side-chain points away from the binding pocket. The side-chain of LysL89 is surrounded by mostly hydrophobic residues: AlaL34, TyrL36, ProL95, PheL98, IleH37, TrpH47, HisH95 and TrpH103, as well as SerL91

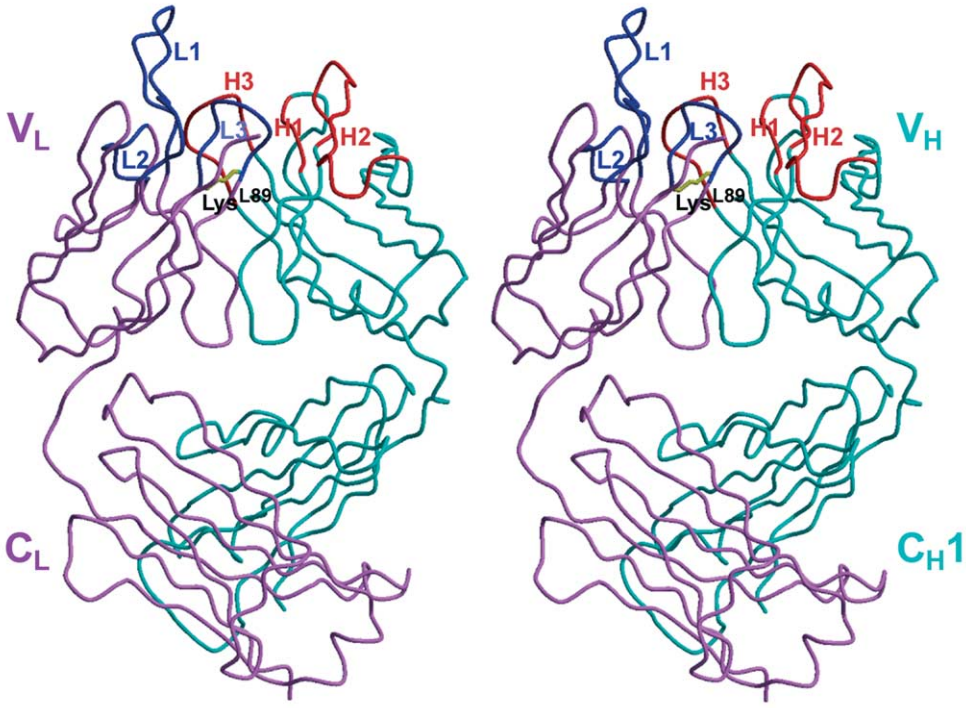

Figure 2. Stereo view of crystal structure of 93F3 Fab′ with the α-carbon trace of the light (L) and heavy (H) chains colored in purple and cyan, respectively; the segments corresponding to the CDR L1, L2 and L3 are colored blue, while the segments corresponding to CDR H1, H2 and H3 are colored red. The reactive lysine LysL89 is also shown in yellow.

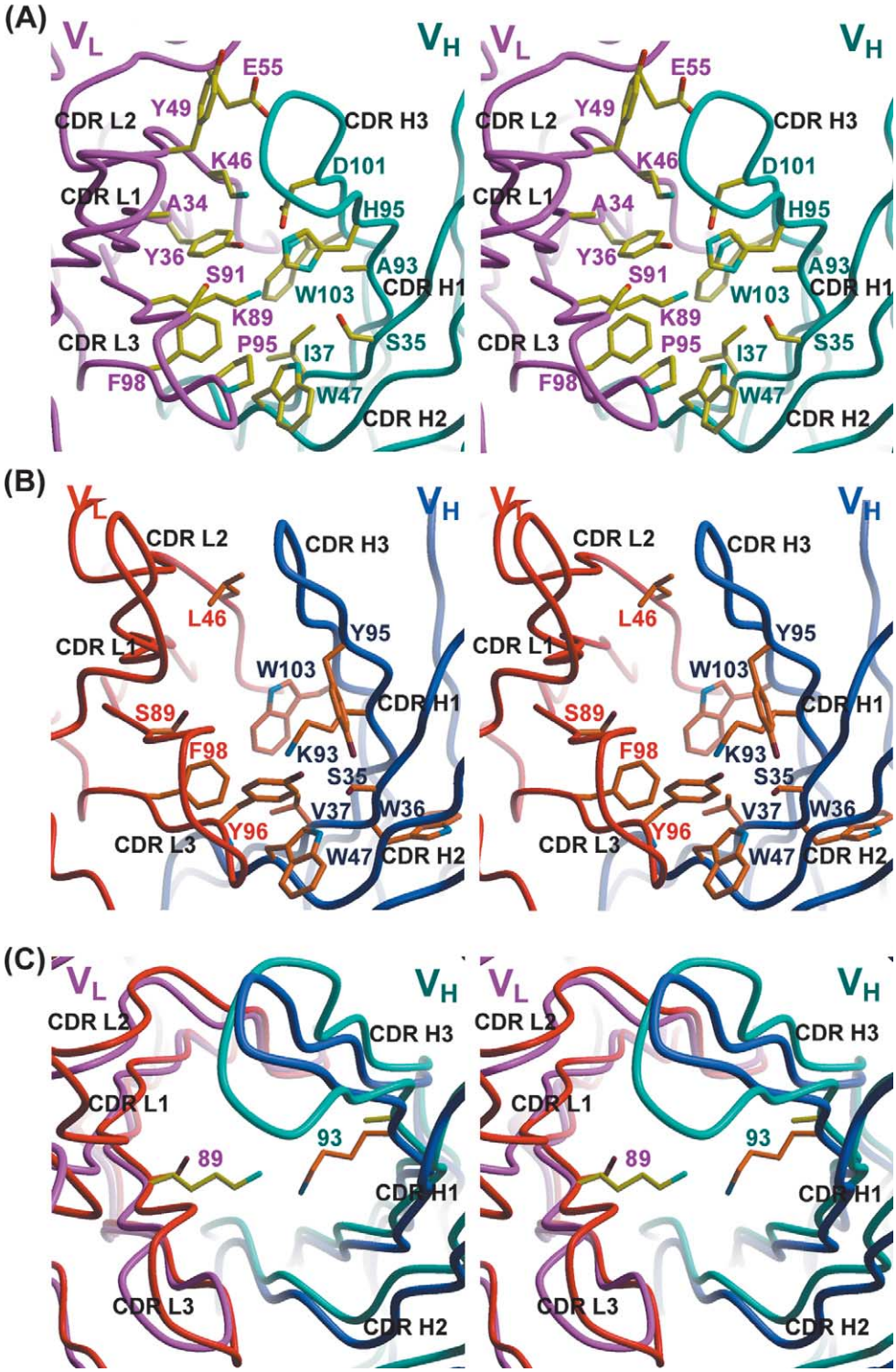

Figure 3. Stereo view of the combining site of antibody 93F3 and comparison with antibody 33F12. (A) Stereo view of antibody 93F3 Fab′ combining site. The side-chains for residues within the vicinity of LysL89 and LysL46 are shown. The light chain is colored in purple and the heavy chain in cyan with the side-chains of the antibody-binding site residues labeled. (B) Stereo view of antibody 33F12 Fab′ combining site.[2] The side-chains for residues within the vicinity of LysH93 are shown. The light chain is colored in red and the heavy chain in blue with the side-chains of the antibody-binding site residues labeled. (C) Comparison of the combining sites of antibodies 93F3 and 33F12. The light and heavy chains of antibody 93F3 are shown in purple and cyan with yellow-carbon side-chains while the corresponding chains of antibody 33F12 are shown in red and blue with brown-carbon side-chains. The side-chains of the active LysL89 of antibody 93F3 and the active LysH93 of antibody 33F12 are in the opposite orientation in the combining sites.

and SerH33. Furthermore, the LysL89 amine does not form hydrogen bonds with nearby residues or water molecules. In contrast, the side-chain of LysL46 is surrounded by mostly hydrophilic residues: GluL55, HisH95 and AspH101, AlaL34, TyrL36, and TyrL49. LysL46 forms a hydrogen bond with a water molecule, but not to nearby residues. Surveys of the Kabat-Wu antibody database[13] reveals these two binding-site lysine residues are rarely found in antibodies. LysL89 occurs in only about 0.64% of antibody sequences in the database, while LysL46 is observed in only 0.067% of antibody sequences. Residue L89 is a glutamine (53.7%) and residue L46 is a leucine (69.4%) in most antibodies. Comparison with known class I aldolase structures shows a similar arrangement of key lysine residues in their active sites, one is directly involved in Schiff base formation and the other functions to perturb the pK_a of the reactive lysine to enhance the efficiency of the aldolase-catalyzed aldol reaction.[14]

To date, the crystal structure of antibody 33F12 Fab is the only other known high-resolution structure of an aldolase antibody (Figure 3(B)).[2] A low-resolution structure of another member of this family, 38C2 Fab, is also available (A.H. *et al.*, unpublished results). Antibodies 38C2 and 33F12 share 92% amino acid sequence identity in their variable domains (only ten and nine substitutions in V_L and V_H, respectively) and have identical CDR lengths. The active LysH93 and six other residues (SerH35, ValH37, TrpH47, TyrH95, TrpH103, and PheL98) that are within a 5 Å radius of its ε-amino group in the structure of 33F12 are completely conserved in both antibodies 38C2 and 33F12 (Figures 1 and 3(B)). As expected, both structures also exhibit a high degree of structural similarity, based on the crystal structure of antibody 33F12 Fab and the low-resolution crystal structure of antibody 38C2 Fab.[8]

Antibodies 93F3 and 33F12 both have a deep cleft between V_L and V_H (Figure 3). The CDR L2, L3, and H2 loops of both structures superimpose quite well, whereas the CDR L1, H2, and H3 loops have clear differences (Figure 3(C)). The CDRs L1 and H3 of 33F12 are one- and two-residues shorter than those of 93F3, respectively, while CDR H2 of 33F12 is three-residues longer than that of 93F3. Most interestingly, the location and orientation of the side-chain of the reactive LysL89 in 93F3 is pseudo-symmetrically disposed across the pseudo-dyad between light and heavy chain compared to that of LysH93 in 33F12 (Figure 3(C)). However, both critical lysine residues are surrounded by mostly hydrophobic residues (Figure 3(A) and (B)). Note that in 33F12, L89 is a serine residue, while in 93F3, H93 is an alanine residue.

Site-directed mutagenesis of antibody 93F3

Consistent with the substrate used in the reactive immunization protocol,[1] the catalytic lysine ε-amino group of the aldolase antibody forms an enamine with the substrate carbonyl in aldolase reactions and forms the enaminone with the diketone along the same reaction coordinate of the aldol reaction. Thus, mutation of the essential lysine residue should lead to the loss of catalytic activity, as well as loss of binding to the diketone.[12,15,16] In order to determine which lysine residue forms the enamine/enaminone, LysL46 and LysL89 of 93F3 were independently substituted with alanine and the binding abilities of these mutants to the diketone were analyzed. Since 93F3 also covalently binds to **1**-BSA, diketone **1** was used in order to simplify the comparison between antibodies 93F3 and 38C2 (or 33F12). LysL46Ala retained the ability to bind to diketone **1**-BSA, while LysL89Ala showed a complete abrogation of binding to diketone **1**-BSA (Table 2), indicating that LysL89 forms the enamine in antibody 93F3.

To analyze the contribution of LysL46 to catalysis, the mutant LysL46Ala was characterized in detail. LysL46Ala bound to diketone **1**-BSA and to diketone **3**[15] (Scheme 1(a)) (K_d = 3 μM) with a K_d value similar to that of wild-type 93F3 (K_d = 1 μM), as determined by inhibition ELISA.[17] The mutant at LysL46Ala also retained retro-aldol activity with substrate **4** (Scheme 1(a) and Table 2), with a k_{cat} 0.039 min^{-1} about 17 times less than that of wild-type 93F3, but with a rate acceleration (k_{cat}/k_{uncat} = 8.7×10^4) well above background and with about 80% of the stabilization energy ($\Delta G = -RT \ln(k_{cat}/k_{uncat})$) of that of wild-type 93F3 for the reaction (Table 2). Furthermore, this mutant retained the wild-type antibody enantiopreference. Mutant LysL46Ala preferentially catalyzed the retro-aldol reaction of (*R*)-**4** over (*S*)-**4** where the ratio of the initial velocities was >99.5 : 1 (at 100 μM of substrate **4**). These results indicate that LysL46 does not have a significant role in the catalytic reaction, as it does not appear to perturb the pK_a of the ε-amino group of LysL89. The surrounding hydrophobic environment must then play the key role for perturbation of the pK_a of LysL89 of 93F3, which is in a hydrophobic environment with no salt bridges or hydrogen bonds to the surrounding protein residues. This scenario is in contrast to natural class I aldolase enzymes, such as DERA[14] and FBP aldolase,[18] which employ an electrostatic mechanism for perturbation of the pK_a of reactive lysine.

Automated docking analyses (see below) also suggest that the hydroxyl group of SerL91 could form a hydrogen bond with carbonyl oxygen of the aldehyde in the transition state of the catalytic reaction. Experiments in a model system for aldolase antibody catalysis suggested that hydrogen bond formation with the reactants in the transition state is important for the catalysis in addition to a requirement for a hydrophobic environment to perturb the pK_a of the reactive lysine.[19] Thus, we prepared the alanine mutant SerL91Ala. This mutant did not bind to the diketone, indicating that SerL91 is critical for the

Table 2. Apparent dissociation constants for diketone **3** and catalytic activity for **4** with the aldolase antibodies

Antibody Fab	Binding with **3**		Retro-aldol reaction for **4**[a]					
	K_d[b] (μM)	$\Delta\Delta G$[c] (kcal/mol)	Substrate	K_m (μM)	k_{cat} (min^{-1})	k_{cat}/k_{uncat}	ΔG[d] (kcal/mol)	Preference[e]
93F3 M/H[f]	1	N/A	(±)-**4**	8 (15[g])	0.66 (2.65[g])	1.5×10^6	−8.4	*R*
93F3 LysL46Ala	3	0.7	(±)-**4**	22	0.039	8.7×10^4	−6.7	*R*
93F3 LysL89Ala	No binding							
93F3 LysL89Ala/AlaH93Lys	10	1.4	(±)-**4**	110	9.7×10^{-3}	2.2×10^4	−5.9	*R*
93F3 SerL91Ala	No binding							
38C2 M/H[f]	0.2	N/A	(±)-**4**	14[g]	1.0[g]	2.2×10^6	−8.7	*S*
33F12 M/H[f]	2	1.4	(±)-**4**	43[g]	0.11[g]	2.4×10^5	−7.4	*S*
38C2 LysH93Ser	10	2.3		–[h]				
38C2 LysH93His	13	2.5		–[h]				
38C2 LysH93Tyr	No binding							
38C2 LysH93Asp	No binding							
38C2 LysH93Ala	No binding							
38C2 SerH100Asp	30	3.0	(*S*)-**4**	150	1.7×10^{-4}	380	−3.5	*S*
38C2 SerL89Lys	30	3.0		–[h]				
38C2 SerL89Lys/LysH93Ser	5	1.9	(*R*)-**4**	800	6.7×10^{-4}	1.5×10^3	−4.3	*R*

[a] K_m and k_{cat} were determined using (±)-**4**, (*R*)-**4** or (*S*)-**4**.
[b] K_d was determined as the concentration of diketone **3** required to inhibit 50% of the maximal binding in the inhibition ELISA. Indication of no binding is based on the ELISA against **1**-BSA.
[c] For mutants of 93F3, $\Delta\Delta G = -RT \ln(K_{d\ 93F3M/H}/K_{d\ mutant})$, and for 33F12 and mutants of 38C2, $\Delta\Delta G = -RT \ln(K_{d\ 38C2M/H}/K_{d\ mutant})$ at 25 °C.
[d] $\Delta G = -RT \ln(k_{cat}/k_{uncat})$ at 25 °C.
[e] Enantiopreference of (*R*)-**4** or (*S*)-**4**.
[f] Mouse–human chimeric Fab produced in *E. coli*.
[g] The data were determined using mouse antibody IgG (values are per active site).
[h] The initial velocity was 400-fold less than that of mouse antibody IgG 38C2-catalyzed reaction when the activity was analyzed using (±)-**4** (200 μM) (per active site).

formation of enaminone with the diketone and accordingly may contribute to the catalytic reaction.

Inversion of enantioselectivity by site-directed mutagenesis

Antibodies 38C2 and 93F3 form the enamine intermediate with LysH93 and LysL89, respectively. In order to explore the chirality of the active sites of aldolase antibodies, the corresponding positions of the catalytic lysine residues were swapped in 38C2 and 93F3.

First, mutants of antibody 38C2 at H93 were examined (Table 2). Since LysH93 is the reactive lysine in 38C2, loss of the binding to diketone and reduction in catalytic rate were expected upon mutation. The LysH93Ala did not bind to diketone as expected; neither did tyrosine nor aspartic acid mutants. Nevertheless, serine and histidine mutants did bind to the diketone with K_ds of 10 μM and of 13 μM, respectively, but since these mutants did not catalyze the retro-aldol reaction of **4**, these substitutions appear to provide hydrogen bonds to the diketone but are incompatible with enaminone formation.

Next, 38C2 mutants SerL89Lys and SerL89Lys/LysH93Ser were prepared (Table 2). SerL89Lys bound to the diketone with a K_d of 30 μM, 150 times higher (lower affinity) than that of wild-type 38C2; the catalytic activity of this mutant was below the detection limit, indicating that introduction of a proximal lysine at L89 decreased rather than increased the catalytic rate. On the other hand, the double mutant SerL89Lys/LysH93Ser, in which the location of the lysine residue was switched from H93 to L89, showed stronger binding ($K_d = 5$ μM) to the diketone than the mutant SerL89Lys. More significantly, the double mutant catalyzed the retro-aldol reaction of **4** with a k_{cat} of 6.7×10^{-4} min^{-1} and a k_{cat}/k_{uncat} of 1500. The k_{cat} value for the double mutant was about fourfold greater than that of a control mutant SerH100Asp. A dramatic difference was observed in the enantioselectivity of the antibody-catalyzed reaction. While the preferred stereoselectiviy of SerL89Lys/LysH93Ser was opposite to that of wild-type 38C2, the double mutant preferentially catalyzed the retro-aldol reaction of (*R*)-**4** and the ratio of the initial velocities of each substrate enantiomer was 95 : 5 for (*R*)-**4**:(*S*)-**4** using the enantiomers of **4** at 200 μM.

For antibody 93F3 (Table 2), the double mutant LysL89Ala/AlaH93Lys showed only a tenfold reduction in diketone binding, and catalyzed the retro-aldol reaction of **4** with a reduced k_{cat} of 9.7×10^{-3} min^{-1} and a k_{cat}/k_{uncat} of 2.2×10^4. However, the enantioselectivity of the reaction catalyzed by this mutation was retained and the ratio of the initial velocities of each substrate enantiomer was 95 : 5 for (*R*)-**4**:(*S*)-**4** (100 μM substrate).

For the antibody-catalyzed aldol reactions, hydrogen bond formation between antibody and reactants may be critical in addition to the lowered pK_a of lysine amino group. Changing the position of the lysine residue from one chain to the other may

change the hydrogen bonds available for stabilization of the catalytic intermediate, which may also be the cause of inversion or retention of enantiopreference of the antibody-catalyzed reactions (also see below).

Computational studies on the enantioselectivity of aldolase antibodies

In order to further investigate the origin of the enantioselectivity of these aldolase antibodies, quantum mechanical and docking calculations of the transition states were carried out for an aldol condensation of acetone **5** and aldehyde **7** to yield β-hydroxyketone **9** (Scheme 1(b)). In the antibody-catalyzed aldol reaction, a lysine ε-amino group initiates a nucleophilic attack on the carbonyl of acetone **5** to form enamine **6** as the intermediate, which then reacts with aldehyde **7** to form β-hydroxyketone. The group of antibodies 38C2 and 33F12 afforded (*S*)-**9** in the aldol reaction and decomposed the same enantiomer in the retro-aldol reaction, and antibodies 84G3 and 93F3 afforded (*R*)-**9** in the aldol reaction and decomposed (*R*)-**9** in the retro-aldol reaction. Thus, the enantioselectivity of the aldol reactions should be determined at the C–C bond forming step.[1–7,12] Kinetic experiments of a chemical aldol reaction *via* an enamine intermediate demonstrated that C–C bond formation is the rate-determining step,[20] and also the enantioselectivity-determining step.

Quantum mechanical calculations with density function theory were carried out to locate the transition state of the rate-determining step. To simplify the calculation, methylamine was used instead of the ε-amine of the essential lysine residue of aldolase antibodies. Four transition states **10**, **11**, **12** and **13** were proposed (Scheme 1(b) and Figure 4). A half-chair six-membered ring with a hydrogen bond between enamine and aldehyde was found in all transition states. Transition states **10** and **11** leading to product (*S*)-**9** have the aryl group at the pseudo-equatorial position and axial position, with activation barriers of 13.8 kcal/mol and 11.5 kcal/mol, respectively. The favorable electrostatic interactions between the methyl group of the enamine and the aryl ring of the aldehyde make **11** more stable than **10**.[21] The (N)H···O distance is 1.59 Å in **10** and the forming C–C bond is 1.94 Å with a contracted C–N bond at 1.30 Å. Transition state **11** has a slightly more compact geometry with the forming C–C bond distance at 1.86 Å. The charges fit from electrostatic potentials in **10** for oxygen, nitrogen and hydrogen are −0.51, +0.41 and −0.68, respectively. Transition state **11** shows a similar charge distribution as **10**. Both **12** and **13** leading to product (*R*)-**9** are the mirror images of **10** and **11**, and energetically equivalent to **10** and **11**, respectively.

Autodock 4.0[22] is the newest version of the docking program based on a hybrid genetic algorithm and allows receptor side-chain flexibility along with a fully flexible substrate (see details in the Computational methods section). As discussed earlier, an antibody reactive lysine residue forms an enamine with a ketone before reacting with an aldehyde. For simplicity, we considered the geometries of the four methylenamine–arylaldehyde transition states in the antibody-catalyzed reactions to be the same as those in the gas phase reactions.

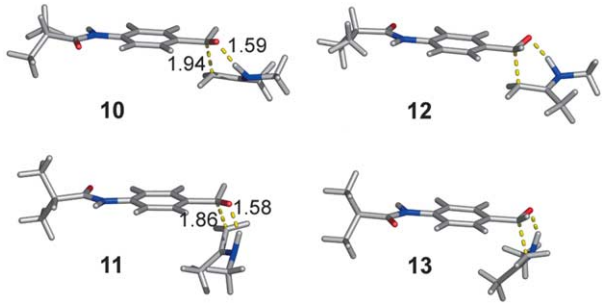

Figure 4. Geometries of four transition states. **10** and **11** lead to (*S*)-**9**, and **12** and **13** lead to (*R*)-**9**. **12** and **13** are the mirror images of **10** and **11**, respectively.

Docking studies of all four transition states show that antibody 33F12 binds **11** and **10**, which lead to product (*S*)-**9** observed experimentally for 33F12,[1,3] with binding free energies of −7.8 kcal/mol and −5.4 kcal/mol, respectively. Furthermore, in the gas phase, **11** is more stable than **10** by 2.3 kcal/mol according to previous quantum mechanical calculations. The combining site of antibody 33F12 with docked **11** is then shown in Figure 5(A). The arylaldehyde moiety sits comfortably in a relatively hydrophobic pocket and the enamine is covalently bonded to LysH93 at the bottom of the binding cavity. Binding free energy analyses also suggest that van der Waals interactions between transition state and surrounding residues contribute most of the binding free energy. The hydroxyl oxygen of TyrL36 is 2.6 Å from the carbonyl oxygen of the aldehyde. Such a hydrogen bond is absent when **12** and **13** are docked in the combining site of 33F12. Docking experiments cannot differentiate **10** and **11** from **12** and **13** purely based on the binding free energies, which could be due to the complicated nature of covalent binding and conformational changes during catalysis. The hydrogen bond between TyrL36 and the aldehyde **7** should be key for the catalysis, as well as for the enantioselectivity of the reaction. TyrL36 is located in framework 2 (FR2) and is conserved in all aldolase antibodies discussed here (Figure 1).

When the location of the active lysine was switched from H93 to L89 in antibody 38C2, the enantiopreference of the catalyzed reaction was reversed (Table 2). SerL89 is located on the other side from LysH93 in the binding pocket, with ample space for SerL89 to be mutated to a bulkier amino acid. As a result, double mutant 38C2 SerL89Lys/LysH93Ser was expected to preserve the combining site structure, except at the positions of the

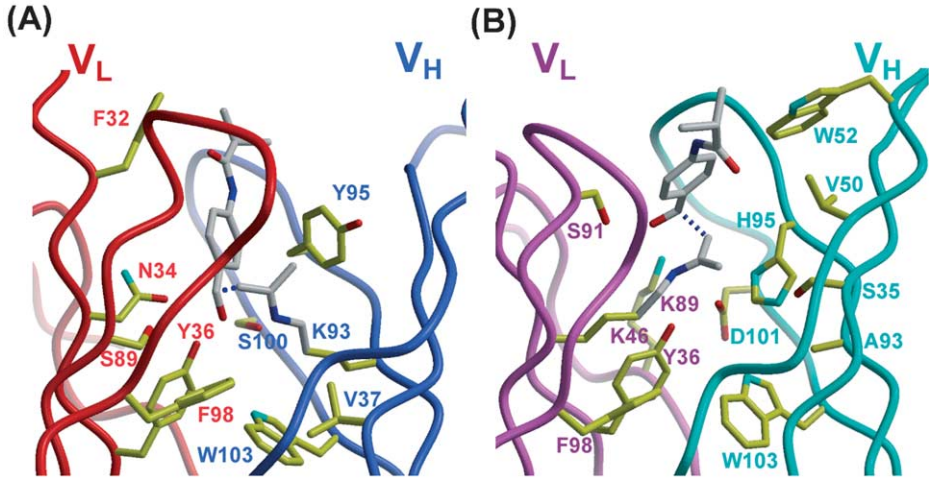

Figure 5. Docked transition states (with gray carbon atoms) in the combining sites of aldolase antibodies. For antibody 33F12, the light chain is colored in red and the heavy chain in blue. For antibody 93F3, the light chain is colored in purple and the heavy chain in cyan. The side-chains for residues within the vicinity of transition states are shown. The ε-amino group of the reactive lysine, LysH93 in 33F12 or LysL89 in 93F3, initiates a nucleophilic attack on the carbonyl of the substrate acetone to form enamine as the intermediate. The nucleophilic attack of enamines on the carbon atoms of acceptor aldehyde groups are shown in blue broken-lines. (A) Docked transition state **11** in the combining site of native antibody 33F12. (B) Docked transition state **13** in the combining site of native antibody 93F3.

mutations. In fact, dockings of all four transition states based on a computational model of 33F12 double-mutant SerL89Lys/LysH93Ser show that **12**, leading to product (*R*)-**9**, has the best binding free energy at −7.6 kcal/mol, which agrees with the observed enantioselectivity of 38C2 double mutant SerL89Lys/LysH93Ser. When **11**, leading to product (*S*)-**9**, was docked into the combining site of this double mutant, no hydrogen bond could be formed between the carbonyl oxygen of the aldehyde of **11** and TyrL36.

Covalent flexible protein docking studies predicted that all four transition states have similar binding free energies at about −8.0 kcal/mol when using the wild-type 93F3 Fab′ crystal structure. According to previous quantum mechanical studies, **13** was more stable than **12** by 2.3 kcal/mol in the gas phase, although both lead to product (*R*)-**9** as experimentally observed for 93F3.[6] The combining site of 93F3 with docked **13** is shown in Figure 5(B). The combining site is relatively narrow compared to that of antibody 33F12. Several side-chains including LysL46, TrpH47, HisH95 and AspH101 are close to LysL89 and **13**. For both **12** and **13**, the carbonyl oxygen of the aldehyde and SerL91 are within hydrogen bonding distance at 2.5 Å. As a proof of this theoretical prediction, antibody 93F3 lost binding to the diketone completely upon SerL91Ala mutation (Table 2). The hydrogen bond between SerL91 and the aldehyde carbonyl oxygen of the transition state thus appears to be critical for the catalysis and can anchor the aldehyde for the enantioselective reaction. Both antibodies 93F3 and 84G3 have the same enantiopreference in the catalyzed reactions and share SerL91 in CDR L3, while aldolase antibodies that have the opposite enantiopreference to 93F3 do not have serine at L91 (Figure 1).

According to the mutation experiment, the double mutant 93F3 LysL89Ala/AlaH93Lys has the same enantiopreference as wild-type 93F3 (Table 2). In comparison to SerL89 of antibody 33F12, AlaH93 of 93F3 is confined in a relatively crowded region (Figure 2(A)). A mutation of 93F3 AlaH93Lys may force a large conformational change in the combining site. Interactions between the 93F3 double mutant and the transition states may thus result in the same enantiopreference. Docking experiments on a computational model of the double mutant 93F3 LysL89Ala/AlaH93Lys did not predict any favorable binding modes for any of the four transition states.

Conclusions

The immune system has provided two groups of aldolase antibodies that catalyze the same aldol reactions, but with antipodal enantioselectivity. The amino acid sequences differ significantly between these two separate groups of antibodies, but with high degree of homology within each group. Structural studies of aldolase antibody 93F3 revealed a combining site with two potential active lysine residues, but subsequent studies showed that LysL89 is the nucleophile that forms the enamine intermediate in the aldol reaction. The other aldolase family represented by antibody 33F12 has one active lysine, LysH93. Antibodies 38C2 and 33F12 use TyrL36, and antibodies 93F3 and 84G3 use SerL91 to form a critical hydrogen bond with the acceptor aldehyde carbonyl oxygen in the transition state of the aldol reactions, respectively. These hydrogen bonds stabilize the transition state of the aldol reactions to afford one of a pair of aldol product enantiomers. That is, the hydrogen bond

interaction activates the acceptor aldehyde carbonyl, fixes the orientation of the aldehyde in the transition state and determines the reaction face of the aldehyde carbonyl. Alternating the location of the reactive lysine residue in antibody 38C2 from H93 to L89 surprisingly resulted in inversion of the enantiopreference of the catalyzed reaction. In the aldolase antibody-catalyzed reaction, the enamine attacks from the *re*- or *si*-face and this facial selectivity appears to depend on the location of the reactive lysine residue and possibly on the identity of the residues forming hydrogen bonds to aldehyde in the transition state.[21]

In the reactive immunization strategy used in the generation of these aldolase antibodies, the catalytic lysine appeared early in the process of antibody evolution from the germline antibody.[2,12] Each group of aldolase antibodies acquired a catalytic lysine residue, but at a different position, while antibodies within the same group originated from the same germline and possessed the same catalytic lysine residue. Once the covalent bond formation event occurred in the immunization process, the binding pocket did not need to evolve further toward higher specificity.[2] For catalysis, hydrogen bond formation between the antibody and the transition state appears to accelerate the reaction rate. During reactive immunization, the hydrogen bond forming residue(s) were effectively selected by enaminone formation with the diketones. When these aldolase antibodies carry out their catalytic reactions, the hydrogen bond interactions generated in the reactive immunization process enhance the aldol reaction rate and determine the enantiopreference.[16] Therefore, these aldolase antibodies can accept a wide range of substrates yet retain their enantiopreference. Thus, the immune system has been used to generate aldolase antibodies that are efficient catalysts with specific enantioselectivity. Careful catalytic antibody design and selection should lead to further improvements in catalytic activity, as well as covalent attachment chemistries between antibody and small molecules.[23] These activities can then be readily exploited in chemical synthesis and drug activation.

Materials and Methods

Determination of amino acid sequences of mouse IgG aldolase antibodies

The antibody variable domain genes from hybridoma cell lines expressing the catalytic antibodies were cloned to pComb3 and sequenced as described.[24]

Crystallization and data collection

Mouse antibody 93F3 Fab′ was produced by standard protocols.[25] The intact 93F3 IgG[6] was digested to $(Fab')_2$ with 14% (w/w) pepsin for seven hours and followed by reduction to Fab′ by incubation with 15 mM L-cysteine for three hours. Protein purification used a combination of protein A and protein G affinity chromatography, as well as ion-exchange chromatography (Mono-S column; Pharmacia).

93F3 Fab′ was concentrated to 16.4 mg/ml in 0.1 M sodium acetate (pH 5.5). Native unliganded Fab′ crystals (Table 1) were grown by the sitting-drop vapor-diffusion method from 16% to 20% (w/v) PEG 8000, 0.3 M zinc acetate, and 0.1 M sodium acetate (pH 5.5). A 2.5 Å data set was collected at the Advanced Light Source on beamline 5.0.2 (ADSC Quantum 4 CCD detector) from a single crystal with 25% (v/v) glycerol as cryoprotectant. The space group is $P2_12_12_1$ with two molecules per asymmetric unit (V_m = 2.56 Å^3/Da, 52% solvent). Data were integrated and scaled with DENZO and SCALEPACK.[26]

Structure determination

The structure of 93F3 Fab′ was determined by molecular replacement methods using the program AMoRe.[27] The coordinates of an Fab fragment of a humanized version of the anti-CD18 antibody H52 (PDB code 2fgw)[28] were used as the search model for rotation and translation function calculations (correlation coefficient = 0.58, R_{cryst} = 0.45 for the resolution range 15.0–4.0 Å). The structural refinement was completed to 2.5 Å resolution with CNS[29] using NCS restraints to give a final R_{cryst} = 0.233 and R_{free} = 0.281 for all data.

Site-directed mutagenesis of antibody 93F3

Site-directed mutagenesis was performed on the 93F3 M/H (mouse–human) chimeric Fab[24] gene in pComb3X by the overlap extension method. Two separate PCR reactions were performed using (i) primer ompseq (5′-AAGACAGCTATCGCGATTGCAG-3′) and the reverse primer indicated below, and (ii) the forward primer indicated below and primer gback (5′-GCCCCCTTAT TAGCGTTTGCCATC-3′). The PCR fragments were then fused using primers ompseq and gback. The fusion PCR product was digested with SfiI and ligated to SfiI-digested pComb3X. The ligation mixture was transformed into *Escherichia coli* TOP10F′. The mutated clones were chosen by sequencing of the variable regions and by ability to bind to goat anti-human IgG $F(ab')_2$ specific antibody in an ELISA against **1**-BSA. The PCR primers used (the mutated codons are underlined) were the following: for 93F3 LysL46Ala mutant, 93F3-L46Ala-b (5′-GTAGATCAATGCTGTAGGAGACTGTCCGGG-3′) and 93F3-L46Ala-f (5′-GGACAGTCTCCTACAGCATTGATC TACTGGGCATC-3′); for 93F3 LysL89Ala mutant, 93F3-L89Ala-b (5′-GGGAAGATCATAAGATTGGGCACAA TAATAAATTGCCAGG-3′) and 93F3-L89Ala-f (5′-GCAATTTATTATTGTGCCCAATCTTATGATCTTCCCA CG-3′); for 93F3 SerL91Ala mutant, 93F3-L91Ala-b (5′-GGAAGATCATAAGCTTGCTTACAATAATAAATTG-3′) and 93F3-L91Ala-f (5′-GTAAGCAAGCTTATGATCTT CCCACGTTCG-3′).

For the double mutant 93F3 LysL89Ala/AlaH93Lys, three separate PCR reactions were performed using (i) ompseq and 93F3-L89Ala-b, (ii) 93F3-L89Ala-f and 93F3-H93Lys-b (5′-GCCGTAGGTATGTTTCTTACAATAGTA CATGGCTGAA-3′), and (iii) 93F3-H93Lys-f (5′-GATT CAGCCATGTACTATTGTAAGAAACATACCTACGGC GG-3′) and gback. The PCR fragments were fused using primers ompseq and gback.

Site-directed mutagenesis of antibody 38C2

For the 38C2 LysH93Ala mutant, PCR reactions using primers (i) ompseq (5′-AAGACAGCTATCGCGATTG

CAG-3′) and H93K/Ala-b (5′-AGAAAATGAG TAAAAATAGGTTGCACAGTAATAAATTCC-3′) and (ii) H93K/Ala-f (5′-GGAATTTATTACTGTGCAACC TATTTTTACTCATTTTCT-3′) and gback (5′-GCC CCCTTATTAGCGTTTGCCATC-3′) were performed. The two PCR fragments were then fused using primers ompseq and gback. The fusion PCR product was digested with SfiI and ligated to SfiI-digested pComb3X.

Antibody 38C2 mutant Fabs (LysH93Ser, LysH93His, LysH93Tyr, LysH93Asp, and SerH100Asp) were prepared using the QuickChange Site-Directed Mutagenesis Kit (Stratagene). Plasmid DNA containing 38C2M/H in pComb3 without the gIII region was used as the PCR template. The following primers were used: LysH93Ser mutant, H93K/Ser-f2 (GTGTATTACTGTAGCACC TATTTTTACTCATTTTC) and H93K/Ser-b2 (GAAAAT GAGTAAAAATAGGTGCTACAGTAATACAC); LysH93-His mutant, H93K/His-f (GTGTATTACTGTCACAYC TATTTTTACTCWTTTTC) and H93K/His-b (GAAAAW GAGTAAAAATAGRTGTGACAGTAATACAC); LysH93-Tyr mutant, H93K/Tyr-f (5′-GGAATTTATTACTGT TATACCTATTTTTACTCATTTTCT-3′) and H93K/Tyr-b (5′-AGAAAATGAGTAAAAATAGGTATAACAGTAA TAAATTCC-3′); LysH93Asp mutant, H93K/Asp-f (5′-GGAATTTATTACTGTGATACCTATTTTTACTCATTT TCT-3′) and H93K/Asp-b (5′-AGAAAATGAGTAAAAA TAGGTATCACAGTAATAAATTCC-3′); SerH100Asp mutant, H100S/Asp-f (5′-CTATTTTTACTCATTTGAT TACTGGGGCCAAG-3′) and H100S/Asp-b (5′-CTTGGCCCCAGTAATCAAATGAGTAAAAATAG-3′).

For the preparation of double mutant 38C2M/H SerL89Lys/LysH93Ser, PCR was performed using L98S/Lys-f (5′-GTTTATTTCTGCAAGCAAGGTACA CATC-3′) as the 5′ primer and L98S/Lys-b (5′-GATGTG TACCTTGCTTGCAGAAATAAAC-3′) as the 3′ primer, and plasmid DNA from the 38C2M/H LysH93Ser mutant in pComb3 without the gIII region as the template.

Mutant protein production and purification

The production of soluble mutant Fab protein was carried out using pComb3 without the gIII region in *E. coli* XL1-Blue cells or using pComb3X in *E. coli* TOP10F′ as described.[24]

Catalytic assay, kinetics, and inhibition ELISA

Catalytic assays were performed in 5% (w/v) DMSO/PBS (pH 7.4). Kinetic determinations and ELISA reactions were performed as described.[15–17]

38C2M/H and 33F12M/H

Mouse–human chimeric Fab was prepared as described.[24] The variable regions of these chimeric Fabs are identical with those of the corresponding mouse antibodies.

Computational methods

All structures were optimized using hybrid density functional theory at the B3LYP/6-31G* level[30,31] with CHELPG[32,33] charges using the Gaussian 98 package.[34] The energies were corrected for zero-point energies.

Autodock 4.0[22] was used for all docking studies. A Lamarckian genetic algorithm (LGA), combining a modified Solis and Wets (SW) local search,[35] was chosen as the primary conformational search method. The population size was 100 with two million energy evaluations. Transition state docking studies on antibody 33F12 were conducted with a rigid receptor antibody. The crystal structure of antibody 93F3 indicated that HisH95 was relatively mobile; therefore, two more degrees of freedom were allowed for the side-chain of HisH95. The reactive lysine residue, LysH93 in 33F12 or LysL89 in 93F3, was modified to an enamine according to the corresponding methylenamine geometry in the gas phase. The aldehyde was then added to the antibody/enamine using the relative positions of enamine and aldehyde in the transition state of the gas phase reaction. One dominant cluster was identified after 100 LGA runs for each case with 1.0 Å root-mean-square deviations.

Swiss PDB Viewer[36] was used to construct the structural models of the 33F12 double mutant SerL89Lys/LysH93Ser and 93F3 double mutant LysL89Ala/AlaH93Lys.

Data deposition

The atomic coordinates and structure factors for the antibody 93F3 Fab′ have been deposited in the RCSB Protein Data Bank with PDB ID code 1T4K. The amino acid sequences of antibodies 93F3 and 84G3 have been deposited in GenBank with accession codes AY532382 (93F3 V_L), AY532383 (93F3 V_H), AY532384 (84G3 V_L), and AY532385 (84G3 V_H).

Acknowledgements

We thank the staff of the Advanced Light Source beamline 5.0.2 for data collection. We also thank Drs Chenglong Li and Garrett M. Morris for helpful discussions on implementing Autodock 4.0. This work was supported by National Institutes of Health grant CA27489 (C.F.B., R.A.L, and I.A.W.) and CA95830 (A.J.O.), and The Skaggs Institute for Chemical Biology. This paper is manuscript no. 16631-MB of The Scripps Research Institute.

References

1. Wagner, J., Lerner, R. A. & Barbas, C. F. (1995). Efficient aldolase catalytic antibodies that use the enamine mechanism of natural enzymes. *Science*, **270**, 1797–1800.
2. Barbas, C. F., Heine, A., Zhong, G. F., Hoffmann, T., Gramatikova, S., Bjornestedt, R. *et al*. (1997). Immune *versus* natural selection: antibody aldolases with enzymic rates but broader scope. *Science*, **278**, 2085–2092.
3. Hoffmann, T., Zhong, G. F., List, B., Shabat, D., Anderson, J., Gramatikova, S. *et al*. (1998). Aldolase antibodies of remarkable scope. *J. Am. Chem. Soc.* **120**, 2768–2779.
4. Zhong, G. F., Shabat, D., List, B., Anderson, J., Sinha, S. C., Lerner, R. A. & Barbas, C. F. (1998). Catalytic enantioselective retro-aldol reactions: kinetic resolution of beta-hydroxyketones with aldolase antibodies. *Angew. Chem., Int. Ed. Engl.* **37**, 2481–2484.
5. Turner, J. M., Bui, T., Lerner, R. A., Barbas, C. F. & List, B. (2000). An efficient benchtop system for multigram-scale kinetic resolutions using aldolase antibodies. *Chem. Eur. J.* **6**, 2772–2774.

6. Zhong, G. F., Lerner, R. A. & Barbas, C. F. (1999). Broadening the aldolase catalytic antibody repertoire by combining reactive immunization and transition state theory: new enantio- and diastereoselectivities. *Angew. Chem., Int. Ed. Engl.* **38**, 3738–3741.
7. Tanaka, F. & Barbas, C. F. (2002). Reactive immunization: a unique approach to catalytic antibodies. *J. Immunol. Methods*, **269**, 67–79.
8. Rader, C., Turner, J. M., Heine, A., Shabat, D., Sinha, S. C., Wilson, I. A. *et al*. (2003). A humanized aldolase antibody for selective chemotherapy and adaptor immunotherapy. *J. Mol. Biol.* **332**, 889–899.
9. Radzicka, A. & Wolfenden, R. (1995). A proficient enzyme. *Science*, **267**, 90–93.
10. Morris, A. J. & Tolan, D. R. (1994). Lysine-146 of rabbit muscle aldolase is essential for cleavage and condensation of the C3–C4 bond of fructose 1,6-bis(phosphate). *Biochemistry*, **33**, 12291–12297.
11. Tanaka, F. (2002). Catalytic antibodies as designer proteases and esterases. *Chem. Rev.* **102**, 4885–4906.
12. Karlstrom, A., Zhong, G. F., Rader, C., Larsen, N. A., Heine, A., Fuller, R. *et al*. (2000). Using antibody catalysis to study the outcome of multiple evolutionary trials of a chemical task. *Proc. Natl Acad. Sci. USA*, **97**, 3878–3883.
13. Kabat, E. A., Wu, T. T., Perry, H. M., Gottesman, K. S. & Foeller, C. (1991). *Sequences of Proteins of Immunological Interest* (5th edit.). National Institutes of Health, Bethesda.
14. Heine, A., DeSantis, G., Luz, J. G., Mitchell, M., Wong, C. H. & Wilson, I. A. (2001). Observation of covalent intermediates in an enzyme mechanism at atomic resolution. *Science*, **294**, 369–374.
15. Tanaka, F., Lerner, R. A. & Barbas, C. F. (2000). Reconstructing aldolase antibodies to alter their substrate specificity and turnover. *J. Am. Chem. Soc.* **122**, 4835–4836.
16. Tanaka, F., Fuller, R., Shim, H., Lerner, R. A. & Barbas, C. F. (2004). Evolution of aldolase antibodies in vitro: correlation of catalytic activity and reaction-based selection. *J. Mol. Biol.* **335**, 1007–1018.
17. Friguet, B., Chaffotte, A. F., Djavadiohaniance, L. & Goldberg, M. E. (1985). Measurements of the true affinity constant in solution of antigen–antibody complexes by enzyme-linked immunosorbent-assay. *J. Immunol. Methods*, **77**, 305–319.
18. Blom, N. & Sygusch, J. (1997). Product binding and role of the C-terminal region in class I D-fructose 1,6-bisphosphate aldolase. *Nature Struct. Biol.* **4**, 36–39.
19. Tanaka, F., Thayumanavan, R., Mase, N. & Barbas, C. F. (2004). Rapid analysis of solvent effects on enamine formation by fluoresence: how might enzymes facilitate enamine chemistry with primary amines? *Tetrahedron Letters*, **45**, 325–328.
20. Reymond, J. L. (1998). Stereoselectivity of aldolase catalytic antibodies. *J. Mol. Catal. B: Enzym.* **5**, 331–337.
21. Bahmanyar, S. & Houk, K. N. (2001). Transition states of amine-catalyzed aldol reactions involving enamine intermediates: theoretical studies of mechanism, reactivity, and stereoselectivity. *J. Am. Chem. Soc.* **123**, 11273–11283.
22. Rosenfeld, R. J., Garcin, E. D., Panda, K., Andersson, G., Aberg, A., Wallace, A. V. *et al*. (2002). Conformational changes in nitric oxide synthases induced by chlorzoxazone and nitroindazoles: crystallographic and computational analyses of inhibitor potency. *Biochemistry*, **41**, 13915–13925.
23. Rader, C., Sinha, S. C., Popkov, M., Lerner, R. A. & Barbas, C. F. (2003). Chemically programmed monoclonal antibodies for cancer therapy: adaptor immunotherapy based on a covalent antibody catalyst. *Proc. Natl Acad. Sci. USA*, **100**, 5396–5400.
24. Barbas, C. F., Burton, D. R., Scott, J. K. & Silverman, G. J. (2001). *Phage Display of Proteins and Peptides: A Laboratory Manual*. Cold Spring Harbor Laboratory Press, Cold Spring Harbor, NY.
25. Harlow, K. U. & Lane, D. (1998). *Antibodies: A Laboratory Manual*. Cold Spring Harbor Laboratory Press, Cold Spring Harbor, NY.
26. Otwinowski, Z. & Minor, W. (1997). Processing of X-ray diffraction data collected in oscillation mode. *Methods Enzymol.* **276**, 307–326.
27. Navaza, J. (1994). Amore—an automated package for molecular replacement. *Acta Crystallog. sect. A*, **50**, 157–163.
28. Eigenbrot, C., Gonzalez, T., Mayeda, J., Carter, P., Werther, W., Hotaling, T. *et al*. (1994). X-ray structures of fragments from binding and nonbinding versions of a humanized anti-CD18 antibody—structural indications of the key role of V(H) residues 59 to 65. *Proteins: Struct. Funct. Genet.* **18**, 49–62.
29. Brünger, A. T., Adams, P. D., Clore, G. M., DeLano, W. L., Gros, P., Grosse-Kunstleve, R. W. *et al*. (1998). Crystallography NMR system: a new software suite for macromolecular structure determination. *Acta Crystallog. sect. D*, **54**, 905–921.
30. Becke, A. D. (1993). Density-functional thermochemistry. 3. The role of exact exchange. *J. Chem. Phys.* **98**, 5648–5652.
31. Lee, C. T., Yang, W. T. & Parr, R. G. (1988). Development of the Colle-Salvetti correlation-energy formula into a functional of the electron-density. *Phys. Rev. B*, **37**, 785–789.
32. Chirlian, L. E. & Francl, M. M. (1987). Atomic charges derived from electrostatic potentials—a detailed study. *J. Comp. Chem.* **8**, 894–905.
33. Breneman, C. M. & Wiberg, K. B. (1990). Determining atom-centered monopoles from molecular electrostatic potentials—the need for high sampling density in formamide conformational-analysis. *J. Comp. Chem.* **11**, 361–373.
34. Frisch, M. J., Trucks, G. W., Schlegel, H. B., Scuseria, G. E., Robb, M. A., Cheeseman, J. R. *et al*. (2001). *Gaussian 98, Revision A.11.1*. Gaussian, Inc., Pittsburgh, PA.
35. Solis, F. J. & Wets, R. J. B. (1981). Minimization by random search techniques. *Math. Oper. Res.* **6**, 19–30.
36. Guex, N. & Peitsch, M. C. (1997). SWISS-MODEL and the Swiss-PDBViewer: an environment for comparative protein modeling. *Electrophoresis*, **18**, 2714–2723.

Edited by R. Huber

(Received 7 June 2004; received in revised form 10 August 2004; accepted 27 August 2004)